Peer-reviewed version available at Energies 2017, 10, , 677; doi:10.3390/en10050677

Electromagnetic Performances Evaluation of an Outer-Rotor Flux-Switching Permanent Magnet Motor Based on Electrical-Thermal Two-Way Coupling Method

Zhengming Shu[1], Xiaoyong Zhu[1,2*], Li Quan[1,2], Yi Du[1], Chang Liu[1]

[1]School of Electrical and Information Engineering, Jiangsu University, Zhenjiang 212013, China

[2]Jiangsu Key Laboratory of Drive and Intelligent Control for Electric Vehicle, Jiangsu University, Zhenjiang 212013, China

shuzhengming90@163.com (Z. S.); quanli@ujs.edu.cn (L.Q.); duyie@ujs.edu.cn (Y.D.); LiuchangAlex49@163.com (C. L.)

* Correspondence: zxyff@ujs.edu.cn; Tel.: +86-159-5287-9732; Fax: +86-511-8878-0088

Abstract: Flux-switching permanent magnet (FSPM) motors have gained increasing attention in the electric vehicles (EVs) applications due to the advantages of high power density, high efficiency. However, the heat sources of both permanent magnet (PM) and armature winding are located on the limited stator space in the FSPM motors, which may result in the PM overheated and irreversible demagnetization caused by temperature rise and it is often ignored in the conventional thermal analysis. In this paper, a new electrical-thermal two-way coupling design method is proposed to analyze the electromagnetic performances, where the change of PM material characteristics under different temperatures is taken into consideration. Firstly, the motor topology and design equations are introduced. Secondly, the demagnetization curves of PM materials under different temperatures are modeled due to PM materials are sensitive to the temperature. And based on the electrical-thermal two-way coupling method, the motor performances are evaluated in details, such as the load PM flux linkage and output torque. Then, the motor is optimized, and the electromagnetic performances between initial and improved motors are compared. Finally, a prototype motor is manufactured, and the results are validated by experimental measurements.

Keywords: electrical-thermal two-way coupling; flux-switching permanent magnet motor; thermal analysis; permanent magnet material characteristics

1. Introduction

With the increasing development of the electric vehicles (EVs), the outer-rotor in-wheel motors have been considered as one of the promising candidates because they can offer the potential superior features of quick torque response, weight reduction, and compact vehicle space [1-4].

Meanwhile, as a key member of stator-PM brushless motors, the flux-switching permanent magnet (FSPM) motors have attracted considerable attention in the EVs applications due to the advantages of high power density, high efficiency [5-8]. In this paper, by incorporating the concept of the outer-rotor in-wheel motor into the FSPM motor, an outer-rotor in-wheel FSPM motor is investigated, where one significant difference of the motor configuration lies in that two permanent magnets (PMs) are artfully placed with V shape in one stator. By the V-shaped placement of adjacent PMs, the flux-focusing effects can be realized, which is able to increase the flux density in the air gap. However, flux-focusing effects may cause the losses of each element easily increased, which further results in the raise of the temperature. In addition, the PMs are embedded in the stator core and surrounded by the concentrated armature windings in the FSPM motor [9-11], both of which are heat sources. The concentrated heat sources may make the PMs overheated and irreversible demagnetization, which inevitably affects the motor performances. Therefore, the thermal analysis, particularly the methods to analyze the electromagnetic performances based on the different PM

Preprints (www.preprints.org) | NOT PEER-REVIEWED | Posted: 4 April 2017 doi:10.20944/preprints201704.0015.v1

Peer-reviewed version available at Energies 2017, 10, , 677; doi:10.3390/en10050677

material characteristics under different temperatures, is an indispensable part in the process of the motor design to ensure the safety operation.

Currently, several methods about thermal analysis have been investigated in the literature. In [12-14], the conventional finite element analysis (FEA) method is applied, it can offer the advantages of simulating complex motor structure and distributed heat sources; however, with the raise of temperature, the change of PM material characteristics is ignored in the method. As a result, the inaccurate results cannot meet the desirable requirements. To obtain accurate results, the iterative parameter method is analyzed in [15], which can efficiently improve the accuracy of the results through multiple iteration calculation. However, the multi-physics simulation is very time-consuming and low efficient, which is inconvenient especially for the complex motor structure. In [16,17], the lumped parameter method is considered as an effective way to realize the thermal analysis because it can offer fast and simple computation and also consider different heat-transfer mechanisms, but just the components' temperature distributions rather than the whole motor are obtained in the method.

In this paper, a new electrical-thermal two-way coupling design method is proposed to analyze the electromagnetic performances based on the investigated FSPM motor, where the change of PM material characteristics under different temperatures is taken into consideration. Firstly, the motor topology is introduced, and the design equations are also deduced. Secondly, the demagnetization curves of PMs under different temperatures are modeled, and by implementing the electrical-thermal two-way coupling method, the load PM flux linkage and output torque are analyzed in details. Then, based on it, the motor is optimized, and the electromagnetic performances between initial and improved motors are compared. Finally, a prototype motor is manufactured and tested for experimental validation.

2. Motor Topology and Design Equation

2.1. Motor Topology

Figure 1 shows the configuration of the 6/22 stator/rotor pole outer-rotor V-shaped flux-switching permanent magnet (V-FSPM) motor. It can be observed that each stator pole of the outer-rotor FSPM motor is embedded two PMs and wound concentrated armature windings, while the rotor pole is simple with 22 iron tooth. Compared with the conventional 12/10 stator/rotor pole FSPM motor [18], the stator pole number of the outer-rotor FSPM motor is reduced by half with only 6 poles. Thus, the stator slot area can be increased under the same dimension size. Meanwhile, the two rectangular PM pieces are purposely placed with V shape in one stator pole, which can enhance the flux-focusing effects and further increase the flux density in the air gap. In addition, the rotor pole is only formed with silicon steel sheets, thus the simple rotor configurations reduce manufacture difficulty and ensure the reliability of the motor, meanwhile, high torque at low speed can be facilitated in the V-FSPM motor due to the high rotor pole numbers arrangement.

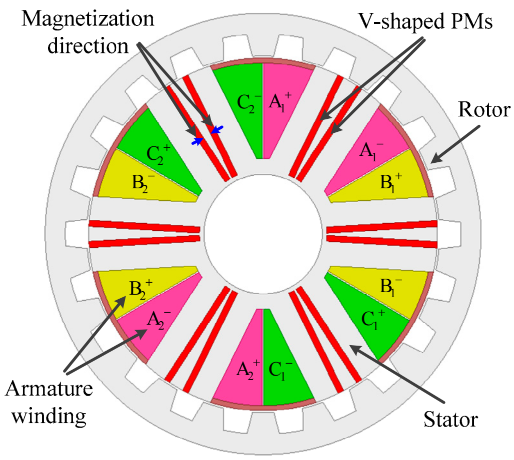

Figure 1. Configurations of the V-FSPM motor.

Peer-reviewed version available at Energies 2017, 10, , 677; doi:10.3390/en10050677

2.2. Design Equations

For the investigated FSPM motor， the feasible combinations of stator and rotor pole numbers can be determined through analysis and calculation. Since the magnetization direction of adjacent PMs is face-to-face, thus, the stator pole number should be even. Meanwhile, the stator pole numbers should be a multiple of the phase number in the three-phase motor. Therefore, the stator pole number should be a multiple of 6. Then, the feasible combinations of stator and rotor pole numbers can be given by:

$$N_s = 6k_1 \quad and \quad N_r = k_2 N_s \pm k_3 \tag{1}$$

where N_r is the number of rotor poles, N_s is the number of stator poles, k_1, k_2 and k_3 are positive integers, it is worthwhile to mention that N_r is preferred to be even number so that the unbalanced magnetic force can be efficiently avoided.

The dimension design of FSPM motor has its inherent standards. Based on the conventional design method, the design equation of the V-FSPM motor can be deduced as:

$$T_{out}(T_{ref}) = \frac{\sqrt{2}\pi^3}{4}\frac{N_r}{N_s} D^2{}_{so} l_a k_s k_d k^2{}_{sio} A_s B_{g\,max} c_s \eta \tag{2}$$

where D_{so} is stator outer diameter, l_a is stack length of the motor, k_s is chute coefficient, k_d is magnetic flux leakage coefficient, k_{sio} is the ratio of inside diameter and outside diameter of the stator, A_s is the line load, B_{gmax} is the peak air gap flux density at no-load condition, c_s is the pole arc coefficient of stator tooth, η is the motor efficiency, T_{ref} is the reference temperature, $T_{out}(T_{ref})$ is the output torque at the reference temperature.

Because the output torque is sensitive to the temperature variation, a temperature scaling factor K_{temp} is introduced, which can be expressed as

$$K_{temp} = \frac{T_{out}(T)}{T_{out}(T_{ref})} \tag{3}$$

where T is temperature, $T_{out}(T)$ is the output torque at the temperature T. In the conventional method, the value of K_{temp} equals to 1 because the temperature impact is ignored. When the temperature rises is considered, the value of K_{temp} is supposed to be less than 1. It can be easily seen that, to obtain high output torque at the temperature T, high value of K_{temp} is needed.

3. Electrical-Thermal Two-way Coupling Method

3.1. Characteristics of PM Material

The permanent magnet materials are sensitive to the temperature, which results in that the PM suffers from performance reduction and even irreversible demagnetization when the motor operates at the high temperature. Therefore, it is necessary to obtain the demagnetization curves of PM materials under different temperatures.

Firstly, the PM intrinsic B_i-H curve at a certain reference temperature is provided by the material supplier, so the remanence and the intrinsic coercive force at the reference temperature can be obtained easily. Based on it, the remanence $B_r(T)$ and the intrinsic coercive force $H_{ci}(T)$ at different temperatures can be derived as

$$\begin{cases} B_r(T) = B_r(T_{ref}) \cdot [1 + \alpha(T - T_{ref})] \\ H_{ci}(T) = H_{ci}(T_{ref}) \cdot [1 + \beta(T - T_{ref})] \end{cases} \tag{4}$$

where $B_r(T_{ref})$ and $H_{ci}(T_{ref})$ are the remanence and the intrinsic coercive force at the reference temperature, α and β are temperature coefficients.

Preprints (www.preprints.org) | NOT PEER-REVIEWED | Posted: 4 April 2017 doi:10.20944/preprints201704.0015.v1

Peer-reviewed version available at Energies 2017, 10, , 677; doi:10.3390/en10050677

Secondly, since the PM intrinsic B_i-H curves at different temperatures have very similar shape, the intrinsic B_i-H curves can be adjusted to one curve (more or less) after the normalized scaling, the normalized intrinsic b_i-h curve can be given by

$$\begin{cases} b_i(T) = B_i(T) / B_r(T) \\ h_i(T) = H_i(T) / H_{ci}(T) \end{cases} \tag{5}$$

where $b_i(T)$ and $h_i(T)$ are the flux density and magnetic field intensity on the normalized intrinsic b_i-h curves at the temperature T. $B_i(T)$ and $H_i(T)$ are the flux density and magnetic field intensity on the original intrinsic B_i-H curves at the temperature T. From equation (5), the normalized intrinsic b_i-h curve at any temperature T can be obtained.

All the intrinsic B_i-H curves at different temperatures are normalized to one curve, thus the normalized intrinsic b_i-h curve applies to all temperatures. To facilitate the calculation, the normalized intrinsic b_i-h curve at the reference temperature is selected. Then, the equation (5) at the reference temperature can be expressed as

$$\begin{cases} b_i(T_{ref}) = B_i(T_{ref}) / B_r(T_{ref}) \\ h_i(T_{ref}) = H_i(T_{ref}) / H_{ci}(T_{ref}) \end{cases} \tag{6}$$

Even though the selected normalized intrinsic b_i-h curve is generated using the reference temperature, it is valid for all temperatures because of the very similar shape. Then the intrinsic B_i-H curves can be given by

$$\begin{cases} B_i(T) = b_i(T_{ref}) \cdot B_r(T) \\ H_i(T) = h_i(T_{ref}) \cdot H_{ci}(T) \end{cases} \tag{7}$$

In this paper, the PM of NdFeB material is employed and the corresponding intrinsic B_i-H curve at the reference temperature (20°C) is provided by the supplier. According to the above analysis, the intrinsic B_i-H curves at different temperatures can be established successfully, which is shown in Figure 2. It can be seen that the temperature variations have important effects on the PM characteristics, and the PM performance reduces when the temperature rises. Therefore, it inevitably leads to the inaccuracy of the analysis results when the temperature rise is ignored, such as distributions of magnetic field, output torque, and efficiency.

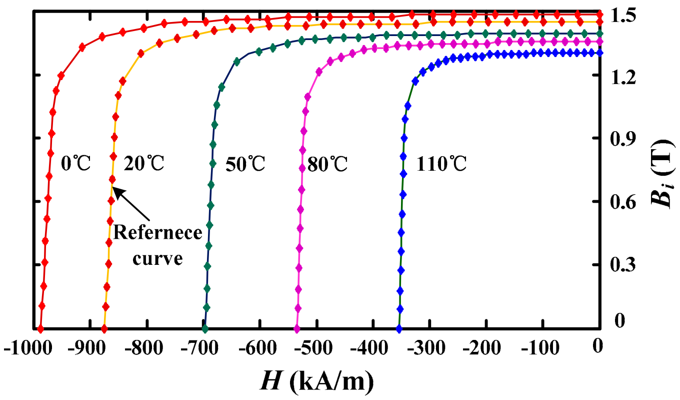

Figure 2. B_i-H curves at different temperatures.

Finally, in the finite element analysis, the required B-H curves of PM can be efficiently transformed from the B_i-H curves in equation (7), the corresponding transformed equation can be expressed as

$$\begin{bmatrix} B \\ H \end{bmatrix} = \begin{bmatrix} 1 & \mu_0 \\ 0 & 1 \end{bmatrix} \cdot \begin{bmatrix} B_i \\ H_i \end{bmatrix} \tag{8}$$

where μ_0 is vacuum permeability.

3.2. The Flow Chart of the Proposed Method

Figure. 3 shows the flow chart of the proposed method. It can be seen that the method mainly consists of the following five steps.

Step 1: Construct the 2-D finite element analysis model and 3-D thermal model according the motor configuration.

Step 2: One way (electrical to thermal way). The losses of each element are respectively calculated in the electromagnetic solver based on the demagnetization curve at the operation temperature. Then, the acquired losses used as the thermal source are imported into the thermal solver, thus the temperature distribution can be obtained. Generally, the results between the obtained temperature and original operation temperature cannot achieve convergence.

Step 3: Another way (thermal to electrical way). The temperature results are fed back to the electromagnetic solver by updating the material properties under the corresponding temperature. Then, the new loss results can be obtained by the electromagnetic performance analysis.

Step 4: Import the new loss results into the thermal solver to get the new temperature distribution. At this time, the temperature convergence can be estimated according to the two temperature results from the thermal solver. If the difference value of the two adjacent temperature results is within the setting threshold, the two-way coupling analysis is completed. Otherwise, it returns back to step 3.

Step 5: Feedback design. Optimize the motor and evaluate the motor's electromagnetic performances. After optimization, if the electromagnetic performances meet the required demands, the motor dimensions can be determined. Otherwise, the dimension parameters need to be further optimized.

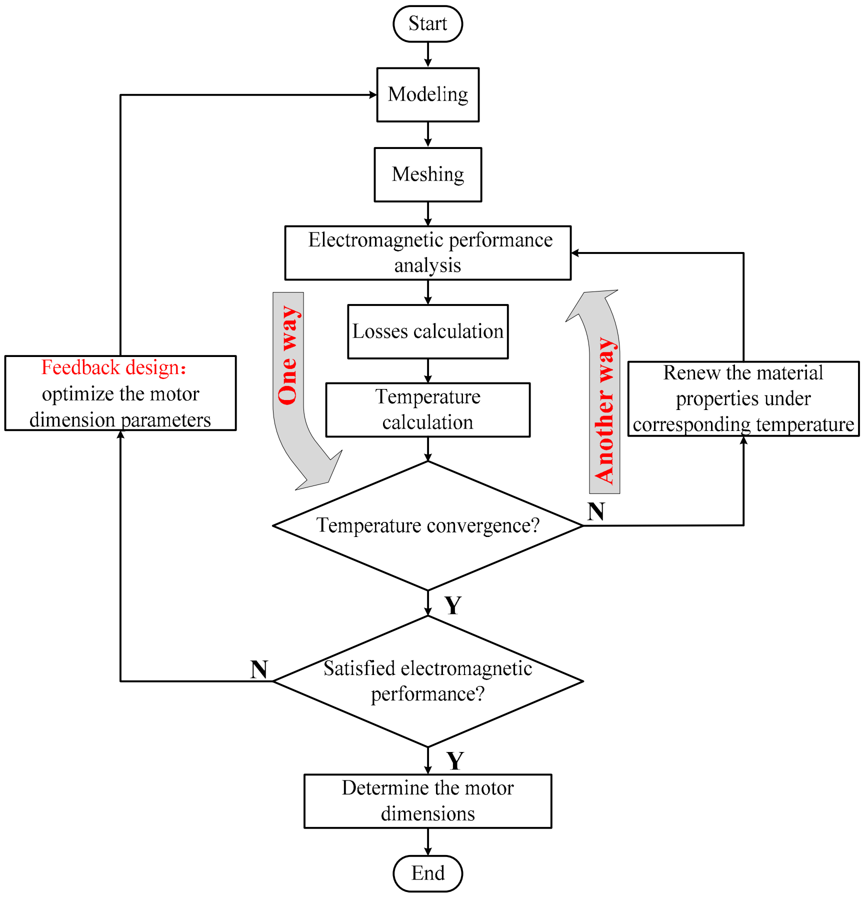

Figure 3. Flow chart of the proposed method.

4. Electrical-Thermal Two-way coupling Analysis

After the introduction of the electrical-thermal two-way coupling method flowchart, the performances and the temperature rise are respectively analyzed in the conventional single-way method (without coupling) and the proposed method (with the electrical-thermal two-way coupling).

The temperature convergence results of two methods are shown in Table 1. It can be seen that the temperature rises with the increase of iteration times and reaches the steady state after multiple

 doi:10.20944/preprints201704.0015.v1

Peer-reviewed version available at *Energies* **2017**, *10*, , 677; doi:10.3390/en10050677

iterations. In the single-way analysis, the temperature reaches the steady state after 20 times iteration, while the two-way coupling analysis reaches the steady state after 40 times iteration. At this time, the convergence temperatures of them are respectively converged with the 86°C and 98°C, indicating that the effect of the temperatures on PM material is effectively considered.

The temperature distributions of the motor by the two methods are shown in Figure 4(a). It can be observed that the temperature with the two-way coupling is higher than that of the conventional single-way method, which indicates that the losses of the motor are increased due to the temperature rise after coupling. Moreover, the highest temperature occurs at the stator teeth due to the concentrated heat sources on the stator. The raise of temperature with coupling will degrade the remanence and the coercive force, which cause the variation of field distribution, especially when the armature current is applied, as shown in Figure 4(b). This will further lead to electromagnetic performances variations, such as load PM flux linkage and output torque.

Table 1. Temperature convergence tracks.

Analysis method		Iteration times						
		0	10	20	30	40	50	……
Single-way	Temperature (℃)	20	85.2	86	86	86	86	86
	Temperature difference (℃)	-	65.2	0.8	0	0	0	0
Two-way coupling	Temperature (℃)	20	86	102	97.3	98	98	98
	Temperature difference (℃)	-	66	16	4.7	0.7	0	0

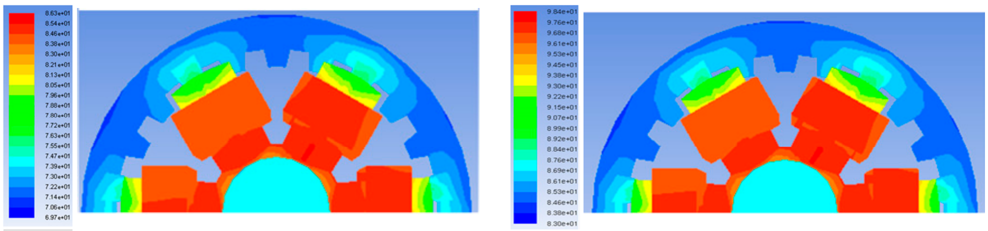

Single-way Two-way coupling

(a)

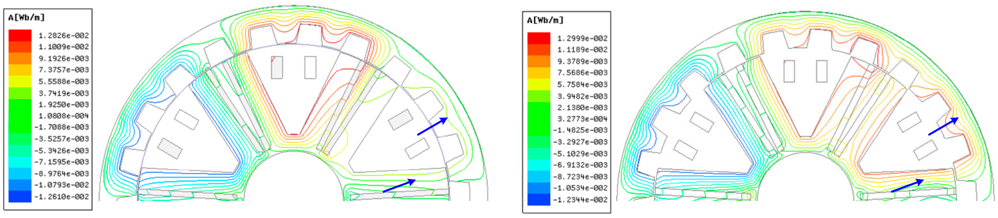

20℃ 98℃

(b)

Figure 4. Comparison results. (a) Temperature distributions. (b) Filed distributions.

Figure 5(a) shows the comparison results of the load PM flux linkage by the two methods. It can be observed that the peak value of the load PM flux linkage is 0.278Wb at the reference temperature 20°C, while the peak value is increased to 0.293Wb at two-way coupling temperature of 98°C, the slightly increase of the load PM flux linkage is resulted by the raise of temperature after coupling, since the iron saturation degree is reduced due to the degraded PM remanence and coercive force when the temperature rises. Figure 5(b) shows the comparison results of output torque. Obviously, due to the temperature rise, the output torque reduced from 26.21Nm to 20.18Nm, which offer a design guide for the following feedback design.

Peer-reviewed version available at Energies 2017, 10, , 677; doi:10.3390/en10050677

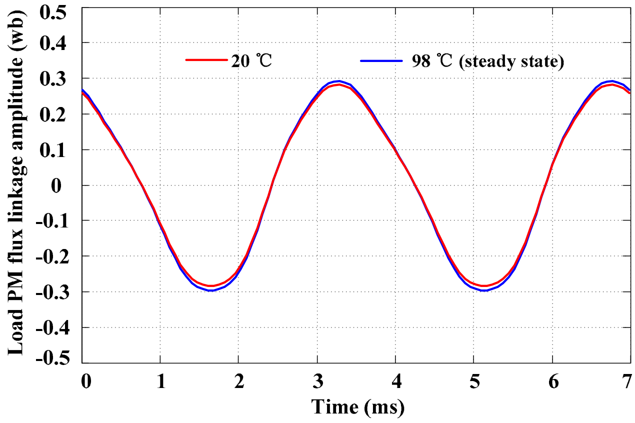

(a)

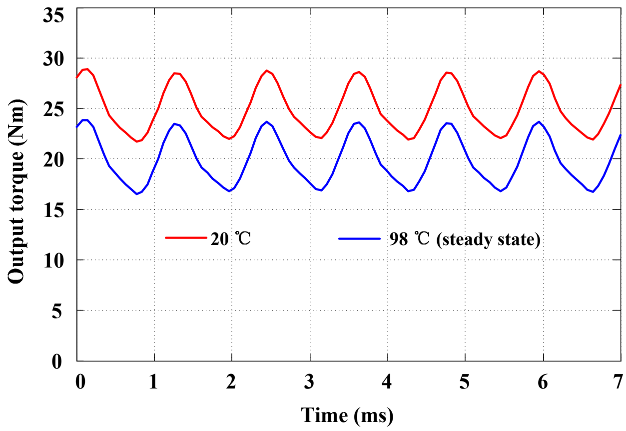

(b)

Figure 5. Comparison results of electromagnetic performances. (a) Load PM flux linkage. (b) Output torque.

5. Motor Optimization

It is illustrated that the aforementioned electromagnetic performances are often degraded during the temperature rise, which results in that the actual performances generally cannot meet the final requirements. Therefore, in order to improve the motor performance accuracy, the feedback design of the V-FSPM motor is needed. According to Figure 3, the feedback design of optimization is implemented after the two-way coupling analysis.

The structure of the investigated V-FSPM motor is relatively complex. As a result, the numbers of motor parameters are relatively large. Considering that rotor tooth width, stator tooth width, PM width and V-shaped angle of two PMs are the leading parameters in design process for the V-FSPM motor and V-shaped angle of two PMs exhibits significant influence on motor performances [19], thus the placed angle of two PMs β_{vs} is selected as a key parameter to be optimized as an example in this section.

In the V-FSPM motor, the V-shaped placement of PMs can enhance the flux-focusing effects and improve the output torque. Since the load PM flux linkage directly affects capacity of the output torque, the relationship between the placed angle of the two PMs β_{vs} and the load PM flux linkage needs to be analyzed. Besides, the cogging torque is an important electromagnetic performance for EVs applications, so the relationship between the placed angle β_{vs} and the peak-to-peak (P–P) cogging torque is also required to be investigated. Figure 6 shows the variation of flux linkage and cogging torque with the change of the angle of the V-shaped PMs. As shown in Figure 6, the cogging torque decreases with the increase of β_{vs} from 2 to 5 degree, and reaches the minimum value when β_{vs} equals to 5 degree. Meanwhile, the load PM flux linkage amplitude possesses a low increase with the raise of β_{vs} from 5 to 7 degree. When β_{vs} increases from 7 to 9 degree, the load PM flux linkage amplitude decreases mainly due to the saturation effect in stator tooth. Considering a compromise design between the high PM flux linkage amplitude and the low

Preprints (www.preprints.org) | NOT PEER-REVIEWED | Posted: 4 April 2017 doi:10.20944/preprints201704.0015.v1

Peer-reviewed version available at Energies 2017, 10, , 677; doi:10.3390/en10050677

cogging torque, β_{vs} is chosen to be 5 degree finally. Then, some key design parameters are listed in Table 2.

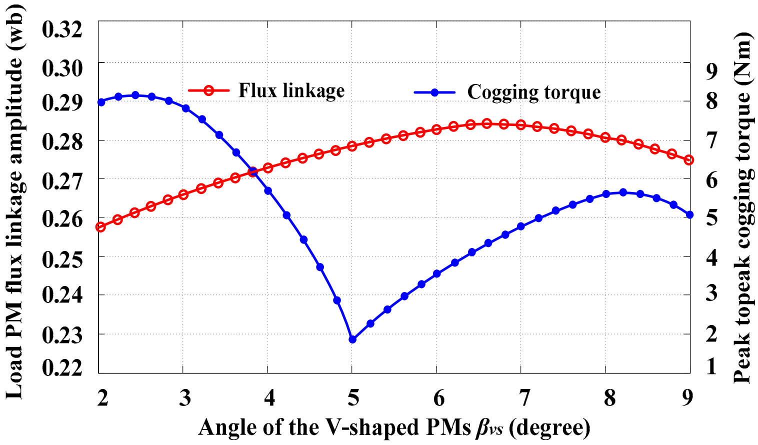

Figure 6. Variation of load PM flux linkage and peak to peak cogging torque with respect to the angle of the V-shaped PMs.

Table 2. Key design parameters

Parameters	Values	Unit
Rotor pole arc width	6	degree
Rotor teeth height	8	mm
Rotor teeth arc width at yoke	10	degree
Air gap length	0.8	mm
Placed angle of the two PMs	5	degree
PM arc width	2	degree
Stator yoke radius	30	mm
Stator yoke arc width	10	degree
Stator inner radius	22.4	mm

Then, Based on the adjusted sizes of the design parameters, the electromagnetic performances of the V-FSPM motor between initial and improved motors are compared in details.

The results with the two-way coupling are shown in Figure 7, including temperature distribution and field distribution. Figure 7 (a) shows the temperature distribution with two-way coupling after optimization. It can be seen that the temperature at the same load current is decreased. Meanwhile, Figure 7(b) shows the field distribution after optimization, the field intensity, after the feedback design, is slightly increased.

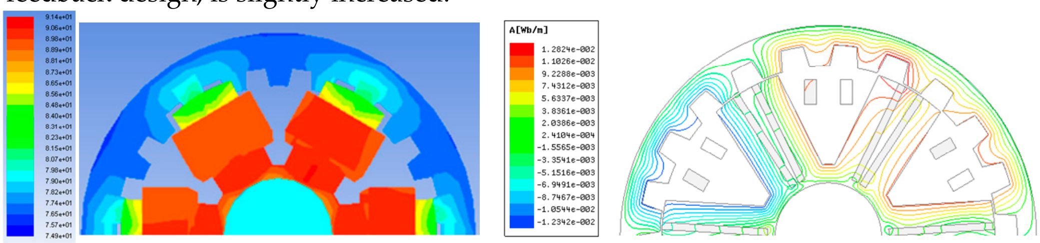

(a) (b)

Figure 7. Optimization results at 91°C after optimization. (a) Temperature distribution. (b) Filed distributions.

The load PM flux linkage waveforms under the initial and improved motors before and after the feedback design are respectively compared, as shown in Figure 8 (a). It can be found that the peak value of the load PM flux linkage after the feedback design is close to the values of initial motor. Figure 8 (b) shows the torque performances of the before and after the feedback design. It can be observed that the output torque after the feedback design at steady-state temperature of 91°C is increased to 22.35Nm, which is increased by 10.75% compared with that before the feedback design. Meanwhile, the initial value of temperature scaling factor K_{temp} is 0.77, higher value of 0.85 is

Peer-reviewed version available at Energies 2017, 10, , 677; doi:10.3390/en10050677

achieved after feedback design, which indicates that the performance of the motor after optimization is efficiently improved. The corresponding comparison results are listed in Table 3.

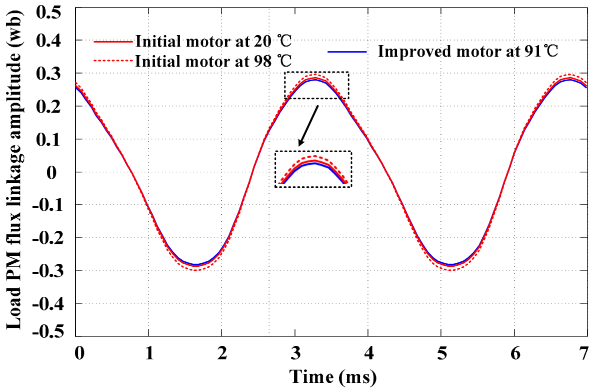

(a)

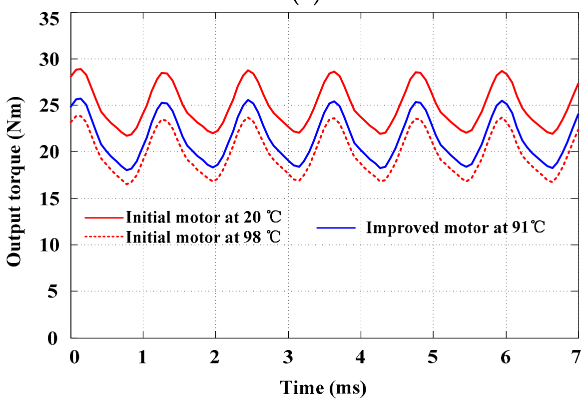

(b)

Figure 8. Comparison results of electromagnetic performances after optimization. (a) Load PM flux linkage. (b) Output torque.

Table 3. Comparisons results

Results	Initial motor at 20°C	Initial motor at 98°C	Improved motor at 91°C
Output torque (Nm)	26.21	20.18	22.35
λ_{temp}	-	0.77	0.85

6. Experiment Validation

In order to further verify the validity of theoretical analysis, a prototype motor is manufactured according to the key design parameters in Table 2. The rotor and stator of the prototype motor are shown in Figure 9 (a) and (b), and the experimental platform can be found in Figure 10. To obtain an experimental validation, the V-FSPM motor is driven continuously with a relatively long period of time to achieve an experiment of temperature rise. In this case, some fundamental experiments of the motor are carried out.

Figure 11 shows the steady-state torque and current waveforms under i_d=0 control method , where T_e, i_a, i_b and i_c represent the waveforms of output torque, phase A, phase B and phase C current, respectively. It can be found that the applied phase current is 11 A, the output torque is 22.15Nm. Meanwhile, the measured torque characteristics under different phase currents are shown in Figure 12. For comparison, the simulated results are also added in this figure. From the figure, it can be seen that the measured torques reasonably agree with the simulated values. The minor discrepancies between the measured and simulated results mainly attribute to manufacturing error such as inaccurate air gap length and V-shaped PM width, the restrictions in experimental conditions and measurement errors. In addition, the variation trends of the output torque at different currents are approximately linear, which implies that the motor possesses desirable over-load capabilities.

Preprints (www.preprints.org) | NOT PEER-REVIEWED | Posted: 4 April 2017 doi:10.20944/preprints201704.0015.v1

Peer-reviewed version available at *Energies* **2017**, *10*, , 677; doi:10.3390/en10050677

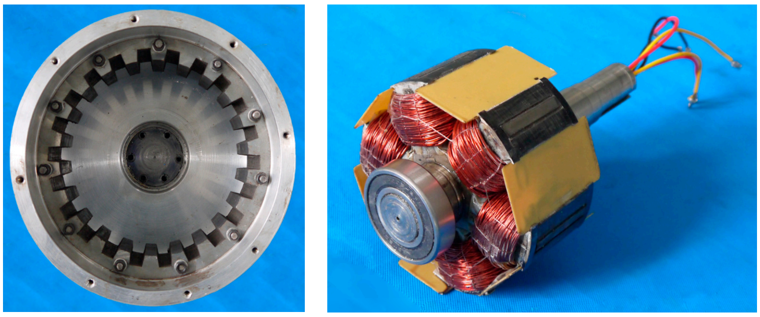

(a) (b)

Figure 9. Prototype motor. (a) Rotor. (b) Stator.

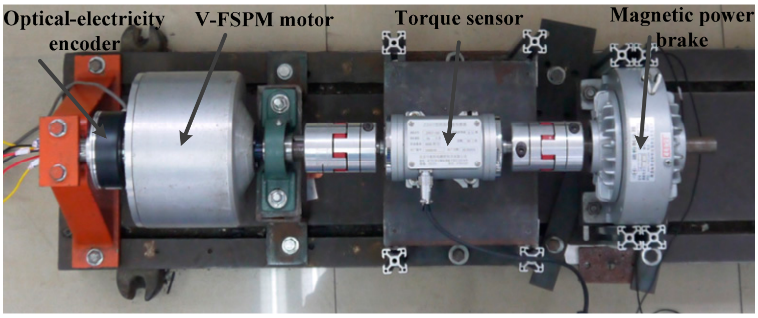

Figure 10. Experimental platforms.

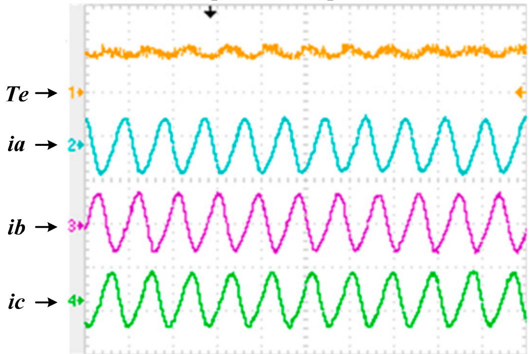

Figure 11. Steady-state torque and current waveforms (25 Nm/div, 15 A/div).

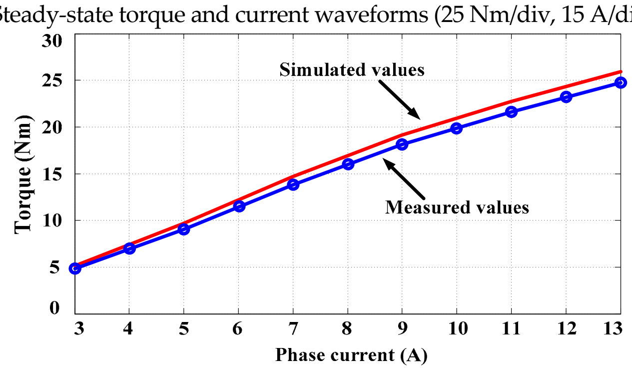

Figure 12. Measured and predicted torque versus different phase currents.

7. Conclusions

This paper proposes a new electrical-thermal two-way coupling design method to analyze the electromagnetic performances, where the change of PM material characteristics under different temperatures is taken into consideration. To illustrate the sensitive degree of PM materials to temperature variation, the demagnetization curves of PMs under different temperatures are modeled. Besides, by implementing the electrical-thermal two-way coupling method, the output torque is reduced obviously compared with the conventional single-way method. Then, Based on the performance characteristics, a feedback design is conducted purposefully through the

 doi:10.20944/preprints201704.0015.v1

Peer-reviewed version available at *Energies* **2017**, *10*, , 677; doi:10.3390/en10050677

adjustment of key design parameters. After the feedback design, the electromagnetic performances between initial and improved motors are compared. Finally, a prototype motor is manufactured to evaluate the performances of the V-PMFS motor. Both the simulation results and the experimental tests validate the correctness of the proposed method.

Acknowledgment: This work was supported by National Natural Science Foundation of China (Grant No. 51477069 and Grant No. 51377073), in part by the Priority Academic Program Development of Jiangsu Higher Education Institutions.

References

1. Chung, S.; Moon, S.; Kim, D.; Kim, J. Development of a 20-Pole–24-Slot SPMSM With Consequent Pole Rotor for In-Wheel Direct Drive. *IEEE Trans. Ind. Electron*. 2016, 63, 302-309.
2. Ifedi, C. J.; Mecrow, B. C.; Brockway, S. T. M.; Boast, G. S. Atkinson, G. J.; D. Kostic-Perovic. Fault-Tolerant In-Wheel Motor Topologies for High-Performance Electric Vehicles. *IEEE Trans. Ind. Appl*. 2013, 49, 1249-1257.
3. Fei, W. Z.; Luk, P. C. K.; Shen, J. X.; Wang, Y.; Jin, M. J. A Novel Permanent-Magnet Flux Switching Machine With an Outer-Rotor Configuration for In-Wheel Light Traction Applications. *IEEE Trans. Ind. Appl*. 2012, 48, 1496-1506.
4. Xue, X. D.; Cheng, K. W. E.; Ng, T. W.; Cheung, N. C. Multi-Objective Optimization Design of In-Wheel Switched Reluctance Motors in Electric Vehicles. *IEEE Trans. Ind. Electron*. 2010, 57, 2980-2987.
5. Cheng, M.; Hua, W.; Zhang, J. Z.; Zhao, W. X. Overview of Stator-Permanent Magnet Brushless Machines. *IEEE Trans. Ind. Electron*. 2011, 58, 5087-5101.
6. Chau, K. T.; Chan, C. C.; Liu, C. H. Overview of Permanent-Magnet Brushless Drives for Electric and Hybrid Electric Vehicles. *IEEE Trans. Ind. Electron*. 2008, 55, 2246-2257.
7. Xiang, Z. X.; Zhu, X. Y.; Quan. L.; Du, Y.; Zhang C.; Fan, D. Y. Multilevel Design Optimization and Operation of a Brushless Double Mechanical Port Flux-Switching Permanent-Magnet Motor. *IEEE Trans. Ind. Electron*. 2016, 63, 6042-6054.
8. Zhu, X. Y.; Xiang, Z. X.; Zhang C.; Quan. L.; Du, Y.; Gu, W. W. Co-Reduction of Torque Ripple for Outer Rotor Flux-Switching PM Motor Using Systematic Multi-Level Design and Control Schemes. *IEEE Trans. Ind. Electron*. 2017, 64, 1102-1112.
9. Lin, T. C.; Zhu, Z. Q.; Liu, K.; Liu, J. M. Improved Sensorless Control of Switched-Flux Permanent-Magnet Synchronous Machines Based on Different Winding Configurations. *IEEE Trans. Ind. Electron*. 2016, 63, 123-132.
10. Zhu, Z. Q.; Chen, J. T.; Pang, Y.; Howe, D.; Iwasaki, S.; Deodhar, R. Analysis of a Novel Multi-Tooth Flux-Switching PM Brushless AC Machine for High Torque Direct-Drive Applications. *IEEE Trans. Magn*. 2008, 44, 4313-4316.
11. Zhang, G.; Hua, W.; Cheng, M.; Liao, J. G.; Wang, K.; Zhang, J. Z. Investigation of an Improved Hybrid-Excitation Flux-Switching Brushless Machine for HEV/EV Applications. *IEEE Trans. Ind. Appl*. 2015, 51, 3791-3799.
12. Li, G. G.; Ojeda, J.; Hoang, E.; Gabsi, M.; Lécrivain, M. Thermal–Electromagnetic Analysis for Driving Cycles of Embedded Flux-Switching Permanent-Magnet Motors. *IEEE Trans. Veh. Technol*. 2012, 61, 140-151.
13. Chen, Y. Y.; Zhu, X.Y.; Quan, L.; Wang, L. Performance Analysis of a Double-Salient Permanent-Magnet Double-Rotor Motor Using Electromagnetic–Thermal Coupling Method. *IEEE Trans. Appl. Supercond*. 2016, 26, 5205305.
14. Li, G. J.; Ojeda, J.; Hoang, E.; Gabsi, M.; Thermal-electromagnetic analysis of a fault-tolerant dual-star flux-switching permanent magnet motor for critical applications. *IET Electr. Power Appl*. 2011, 5, 503–513.
15. Sun, X. K.; Cheng, M.; Zhu, S.; Zhang, J. Z. Coupled Electromagnetic-Thermal-Mechanical Analysis for Accurate Prediction of Dual-Mechanical-Port Machine Performance. *IEEE Trans. Ind. Appl*. 2012, 48, 2240-2248.
16. Thomas, A. S.; Zhu, Z. Q.; Li, G. J. Thermal Modelling of Switched Flux Permanent Magnet Machines. *In Proc. 21st Int. Conf. Electr. Mach*.(ICEM'14). Berlin, Germany, 2-5 September 2014; pp. 2212 – 2217.
17. Cai, X. H.; Cheng, M.; Zhu, S.; Zhang, J. W. Thermal Modeling of Flux-Switching Permanent-Magnet Machines Considering Anisotropic Conductivity and Thermal Contact Resistance. *IEEE Trans. Ind. Electron*. 2016, 63, 3355-3365.

Peer-reviewed version available at *Energies* **2017**, *10*, , 677; doi:10.3390/en10050677

18. Cao, R.W.; Mi, C.; Cheng, M. Quantitative Comparison of Flux-Switching Permanent-Magnet Motors With Interior Permanent Magnet Motor for EV, HEV, and PHEV Applications. *IEEE Trans. Magn*. 2012, 48, 2374-2384.
19. Zhou, Y. J.; Zhu, Z. Q. Torque Density and Magnet Usage Efficiency Enhancement of Sandwiched Switched Flux Permanent Magnet Machines Using V-Shaped Magnets. *IEEE Trans. Magn*. 2013, 49, 3834-3837.